







## Electrical measurement of the spin Hall effect isotropy in ferromagnets with strong spin-orbit interactions

M. Cosset-Chéneau <sup>1,\*</sup>, M. Husien Fahmy <sup>1</sup>, A. Kandazoglou,<sup>1</sup> C. Grezes,<sup>1</sup> A. Brenac,<sup>1</sup> S. Teresi,<sup>1</sup> P. Sgarro,<sup>1</sup> P. Warin <sup>1</sup>,  
A. Marty <sup>1</sup>, V. T. Pham <sup>1,2</sup>, J.-P. Attané <sup>1</sup> and L. Vila<sup>1,†</sup>

<sup>1</sup>Université Grenoble Alpes, CEA, CNRS, INP-G, Spintec, F-38054 Grenoble, France

<sup>2</sup>IMEC - Leuven, 3001 Belgium



(Received 20 May 2022; revised 14 August 2022; accepted 29 November 2022; published 15 December 2022)

The spin-dependent transport properties of paramagnetic metals are roughly invariant under rotation. By contrast, in ferromagnetic materials, the magnetization breaks the rotational symmetry, and, thus, the spin Hall effect is expected to become anisotropic. Here, using a specific design of lateral spin valves, we measure electrically the spin Hall effect anisotropy in ferromagnetic NiCu and NiPd. We show that the magnetization vector does not lead to a sizable anisotropy of the spin charge interconversion and spin transport parameters in materials with a spin-orbit coupling comparable to the exchange interaction.

DOI: [10.1103/PhysRevB.106.L220405](https://doi.org/10.1103/PhysRevB.106.L220405)

Spintronics is primarily based on the exchange interaction between the spins of conduction electrons and the local magnetization in ferromagnets (FMs). This interaction is fundamental in effects such as the giant magnetoresistance [1] and the spin transfer torque [2]. More recently, the use of spin orbit (SO) interactions to manipulate spins in nonmagnetic materials has triggered the birth of spinorbitronics, a new subfield of research and technology aimed at developing new spintronics devices based on SO effects, such as the SOT-MRAM [3] or the magnetoelectric spin-orbit devices [4].

The main SO effect used in spinorbitronics is the spin Hall effect (SHE) [5] that allows the conversion of a spin current into a charge current. So far, the study of the SHE has been mostly focused on nonferromagnetic systems, such as semiconductors [6] and heavy metals [5].

Recent experiments and theoretical calculations have, however, shown that beyond their usual role for spin current injection [7,8] and detection [1,8–10] through exchange coupling, FMs possess an interesting potential for spin-charge interconversion [11–15]. The presence of the magnetization in these materials raises a fundamental question as it breaks the rotational symmetry [16]. The SHE in FMs is, therefore, expected to be anisotropic, i.e., it should depend on the relative orientation between the magnetization and the applied charge current [17].

The rare observations of this anisotropy have been performed in  $3d$  elements below the Curie temperature but show different results for similar materials with a moderate anisotropy in Py [18], a large one in CoFe [19], and an isotropic behavior in Co [20]. This could result from differences in-between material properties, but also from the fact that a precise measurement of this anisotropy remains

challenging. The main techniques used to measure the SHE in heavy metals are spin pumping [21], local [22], and nonlocal (NL) [23] transport in nanostructures, spin Hall magnetoresistance [24], spin Seebeck effect [25], and spin-orbit (ST) torque techniques, such as ST-ferromagnetic resonance [9] or second harmonic [26]. Observing the SHE anisotropy in FMs using these methods is, however, not straightforward as it requires controlling independently the magnetization of two different FMs in direct contact [20,27–31]. Techniques involving a charge current flowing into the FM-SHE material are made complicated by contamination from spurious effects, such as the planar Hall effect [32] and the anomalous Hall effect [33], whereas the methods based on nonlocal magnon transport that allowed for the observation of an anisotropic SHE in FMs [18,19] involve the direct contact between the magnetic insulator and the studied FM material, which could render complex the interpretation of these results [34].

Here, we propose a new design of lateral spin valves, which provides a way to measure the anisotropy of the SHE in FMs. We use it to measure this anisotropy in NiCu and NiPd, which have been found to exhibit spin Hall angles (i.e., the charge to the spin conversion rate) similar to those of the best heavy metals [27,35,36]. The low Curie temperature of these materials allows performing the measurements either in the paramagnetic or ferromagnetic phase. In both cases, the measured inverse spin Hall effect signal is found to be independent from the magnetization direction, the observed variations being smaller than our measurement precision of 10%. These results demonstrate that in these materials the breaking of symmetry due to the ferromagnetic order does not lead to a significant anisotropy of the SHE.

The measurements are based on the injection of a charge current from the injecting CoFe electrode towards one branch of the copper channel [cf. Fig. 1(b)]. This creates a pure spin current flowing towards the detecting electrode [Fig. 1(a)]. The device can be studied using two different measurement configurations. The NL spin signal configuration consists in detecting the voltage drop in between the detecting electrode

\*Current address: Physics of Nanodevices, Zernike Institute for Advanced Materials, University of Groningen, 9747 AG Groningen, The Netherlands; m.n.c.g.cosset-cheneau@rug.nl

†laurent.vila@cea.fr

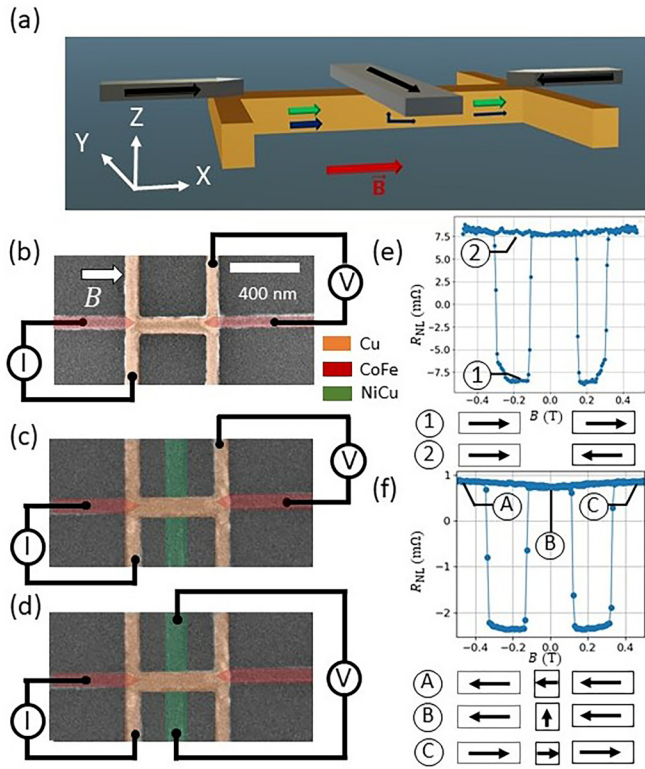


FIG. 1. (a) Device geometry with the FM parts in gray and the Cu in orange. The black arrows in the FM parts represent the magnetization directions. The dark blue and green arrows within the channel represent the spin current flow direction and its polarization, respectively. The LSV has been represented with the FMs on top for the sake of clarity, but in the actual device they lie below the Cu channel to ensure well-defined micromagnetic configurations within the electrodes and in the absorber. (b) Colored SEM image of a reference LSV without the absorber, in the NL measurement configuration. (c) Colored SEM image of a LSV with the absorber, in the NL measurement configuration. (d) Colored SEM image of a LSV in the inverse SHE (ISHE) measurement configuration. (e) NL signal at 12 K for a reference LSV, and (f) with a 100-nm-wide NiCu absorber.

and the channel. By reversing the magnetization of the injecting electrode using an external magnetic field along the easy magnetization axis, it is possible to change the polarization direction of the spin current. This leads to two different nonlocal voltages, high (1) and low (2) at the detecting electrode [Fig. 1(e)]. By comparing this signal with that of a device with absorber [Figs. 1(c) and 1(f)], it allows measuring the spin current flowing towards the absorber [37]. It is then possible to use the ISHE measurement configuration [Fig. 1(d)] in which the spin current is partly absorbed by the SHE absorber. The polarization of the absorbed spin current is along  $X$ , whereas, the absorbed spin current direction flows along the  $Z$  axis. It, thus, generates in the ferromagnetic SHE absorber an electric field along  $Y$  and, consequently, an ISHE signal at the extremities of the absorber.

When applying small fields along  $X$ , the magnetization of the ferromagnetic SHE absorber rotates, whereas the magnetization of the electrodes remain along  $X$ . It is, thus, possible to control the angle in between the polarization direction of the

absorbed spin current and the magnetization of the absorber [38]. Then, if one applies large enough magnetic fields along  $X$ , the magnetization of the injecting electrode reverses. The polarization of the injected spin current is then reversed. This causes a sign change in the ISHE signal/spin signal, allowing to measure the ISHE/spin signal amplitude.

The main advantage of this detection scheme with respect to methods based on LSVs [11,39] is the possibility to control independently the magnetization direction of the electrodes and of the absorber, moreover, using very small fields, in order to avoid field-induced contributions, such as the Hall or Hanle effects [40,41].

We used CoFe injecting and detecting electrodes, and Cu for the copper channel in order to take advantage of its long spin-diffusion length and small interface resistance with CoFe [8,42]. A control sample has also been realized using a platinum absorber [38] as Pt is a well-known material [43]. Then, the measurements of the SHE anisotropy were performed in devices with absorbers made of NiCu and NiPd, two low  $T_c$  FMs with strong SO interactions.

The devices were fabricated by conventional lithography techniques [37]. The magnetoresistance measurements have been performed using lock-in techniques ( $I = 400 \mu\text{A}$ ,  $f = 123 \text{ Hz}$ ). The nonlocal signal measured in a reference lateral spin valve (LSV) without an absorber [Fig. 1(b)] is larger [Fig. 1(e)] than the one detected in a device with a NiCu absorber [Figs. 1(d) and 1(f)] with a signal amplitude going from 15 to  $3.3 \text{ m}\Omega$ . This NL signal difference allows measuring the spin conductance of the absorbing SHE wire and, thus, evaluating the amount of spin current absorbed by the ferromagnetic ISHE material [38].

In the device presented in Fig. 2(a), we performed both nonlocal measurements [cf. Fig. 1(c)] and ISHE measurements [Fig. 1(d)] with an ISHE signal amplitude of  $120 \mu\Omega$ . Contrary to what can be obtained using classical LSVs with FM materials [11], the signals can here be measured at low fields, allowing the control of angle  $\phi$  in between the absorber magnetization and the spin current polarization [cf. Fig. 2(b)]. At low fields, the magnetization of the absorber is along  $Y$  and, thus, transverse to the spin current polarization, which is along  $X$ . At high fields, the magnetization of the absorber is along  $X$  and, thus, collinear to the spin current polarization.

Let us first focus on the nonlocal measurements. Using the measurement configuration of Fig. 1(c), clear nonlocal signals can be obtained for devices with NiCu absorbing wire, both in the ferromagnetic and in the paramagnetic phase [cf. Fig. 2(c)].

Adding the absorbing NiCu wire to the LSV leads to a strong decrease in the nonlocal signal [cf. Figs. 1(e) vs 1(f)]. The presence of the absorbing wire between the injecting and detecting CoFe electrodes indeed leads to a partial absorption of the spin current flowing into the channel. The absorbed spin current is denoted  $j_z^x$  as it flows in the  $Z$  direction and has a spin polarization along  $X$ . Its expression is given by the relation [10],

$$j_z^x = G_{\text{eff}}(\mathbf{m})\mu^x, \quad (1)$$

with  $\hat{m}$  as the magnetization direction of the absorber and  $\mu^x$  as the spin accumulation along the  $x$  direction at the interface between the Cu channel and the absorber.  $G_{\text{eff}}$  is treated as an

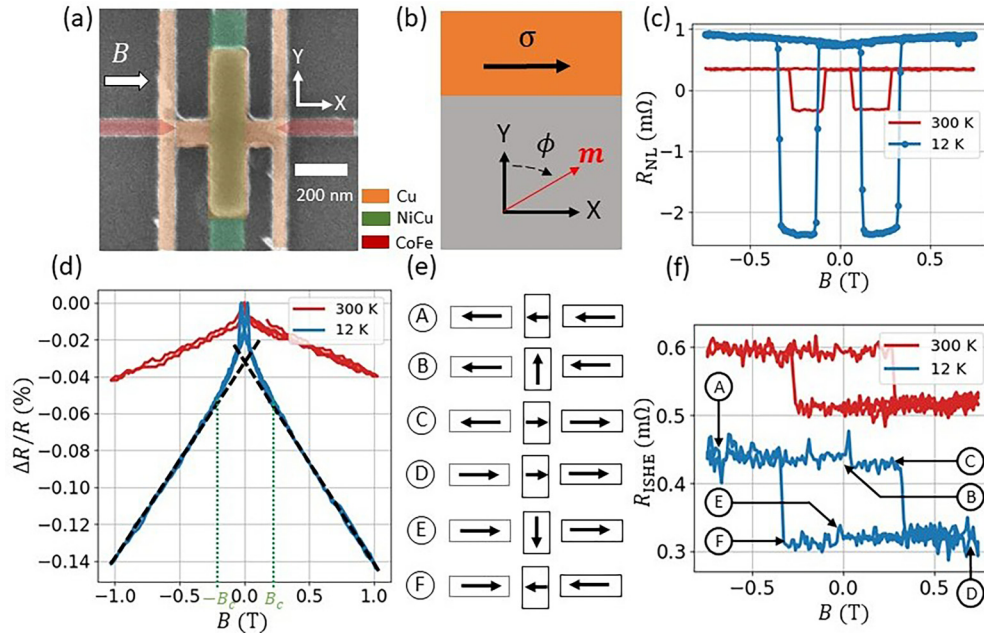


FIG. 2. (a) Colored SEM image of a LSV with a NiCu absorber. The central part of the device is additionally covered with a Cu thin film to avoid spurious magnetoresistive contributions to the signal [38]. (b) Relative orientation between the spin current polarization  $\sigma$  and the magnetization of the absorber at low ( $\phi = 0$ ) and high ( $\phi = \pi/2$ ) fields. (c) NL signal at room temperature (red) and at 12 K (blue) using a 100-nm-wide NiCu absorber. (d) Two-probe magnetoresistance of the 100-nm-wide NiCu absorber measured at 12 K (blue) and at room temperature (red) for a magnetic field transverse to its easy magnetization axis. (f) ISHE measurement in a NiCu absorber, made simultaneously to the NL measurement shown in (c), and (e) scheme of the corresponding magnetic configurations.

effective parameter taking into account the spin conductance  $G_s = 1/\rho l_{sf}$  with  $\rho$  and  $l_{sf}$  as the resistivity and spin-diffusion length of the absorbing material [44] (for  $\mathbf{m} = \hat{x}$ ) or the spin mixing conductance  $G_{\uparrow\downarrow}$  ( $\mathbf{m} = \hat{y}$  or  $\hat{z}$ ) [44,45] as well as the interface resistance  $R_{int}$ .

We extracted from the NL signals  $G_{eff}$  and, thus,  $j_z^x$  at the NiCu/Cu interface using finite element method simulations [8] (see Ref. [38] for computation details and extracted parameters). As seen in Fig. 2(c), the nonlocal signal at 12 K and, thus, the absorbed spin current is found to be relatively independent on the relative angle between the spin polarization and the absorber magnetization [38]. This absence of modulation, which contrasts with the results obtained in Ref. [44] using Py, Co, and CoFe as ferromagnetic absorbers, is possibly due to the relatively high interface resistance ( $7 \text{ f}\Omega \text{ m}^2$ ) between Cu and NiCu [38] when compared to the minimal Sharvin interfacial resistance at the copper 3d-FM interface ( $0.8 \text{ f}\Omega \text{ m}^2$ ) [44]. The modulation being smaller than the experimental error bar, the values of the spin conductance and of the effective spin mixing conductance can be considered to be equal.

Now that the absorbed spin current is known, let us focus on the ISHE. We first measured the dependence of the magnetization direction of the NiCu SHE absorber as a function of the field applied along  $X$  by performing two probe magnetoresistance measurements of the NiCu wire [Fig. 2(d)]. The magnon magnetoresistance contribution [46,47] dominates the signal in both the paramagnetic and the ferromagnetic phases. In the ferromagnetic phase, the magnetoresistance also displays at low fields a deviation from the linear behavior, corresponding to the expected anisotropic magnetoresistance.

This allows measuring the saturation field of the NiCu wire ( $B_c = 0.2 \text{ T}$ ) along the  $X$  axis ( $\phi = \pi/2$ ).

We then measured the ISHE signal using the configuration of Fig. 1(d) at both 12 and 300 K. The Curie temperature of  $\text{Ni}_{60}\text{Cu}_{40}$  has been found to be around 220 K for this composition [27]. Using the nonlocal and ISHE measurements, we extracted an effective spin Hall angle (2.3%), consistent with the one of Ref. [27] measured using spin pumping, which confirms the validity of our measurement method [38]. The ISHE signal, shown in Fig. 2(f), is a square loop in both the paramagnetic and the ferromagnetic phases. The observed square loops reflect the change in sign of the absorbed spin current polarization when reversing the injector magnetization. The symmetry and shape of the signal correspond to what can be expected from the ISHE symmetries and from the switching fields measured in the nonlocal configuration. The parallel and transverse ISHE signals can then be obtained as  $\Delta R_{ISHE}^{\perp} = R^B - R^E$  and  $\Delta R_{ISHE}^{\parallel} = R^A - R^D$ ,  $R^i$  being the electric potential drop in the magnetic state  $i$  reported in Fig. 2(e). The key finding is that at 12 K, the ISHE signal is constant in the  $[-0.2; 0.2 \text{ T}]$  field range where the magnetization of the absorber rotates from the  $X$  to the  $Y$  direction so that  $\Delta R_{ISHE}^{\perp} = \Delta R_{ISHE}^{\parallel}$ . This means that the ISHE is independent of the direction of the absorber magnetization. This isotropy of the ISHE in the ferromagnetic phase is also illustrated by the fact that very similar loops in shape are observed in the paramagnetic phase where one does not expect any anisotropy and in control devices using Pt as absorber [38].

We also performed similar measurements using a 15-nm-thick  $\text{Ni}_{16}\text{Pd}_{84}$  ferromagnetic absorber in which the origin of the ISHE is extrinsic [35] whereas it is intrinsic in NiCu



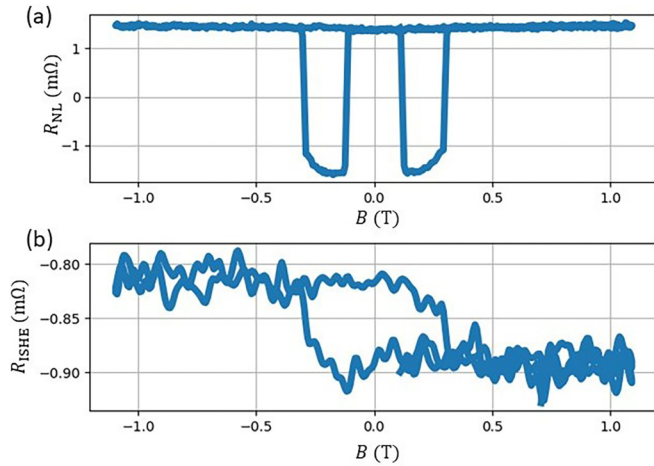


FIG. 3. (a) Nonlocal and (b) ISHE signals measured during the same magnetic-field sweep at 150 K with a 15-nm thick NiPd absorber.

[27]. This alloy is ferromagnetic below 230 K. It has an out-of-plane magnetization at low temperature [38] but in plane above 150 K [cf. Fig. 3(c)]. In order to avoid the strain-induced magnetic inhomogeneity associated with an out-of-plane magnetization in this material [48], we measured the ISHE and nonlocal signal at 150 K when NiPd is still magnetic and its magnetization is in plane. Similar to the case of NiCu, the ISHE signal is found to be isotropic with respect to the magnetization direction.

The ISHE, thus, appears to be isotropic both for NiCu and NiPd in their ferromagnetic phase. This result is very surprising as there is a symmetry breaking induced by the appearance of the magnetization at the paramagnetic/ferromagnetic transition. Theoretical studies have indeed predicted a sizable modulation of the interconversion when rotating the magnetization [17,49], which would be expected to be especially large [13] for materials, such as NiCu and NiPd with large anomalous Hall angles (2% and 4%, respectively) compared to their SHE angles (2.3% and 1% [38]).

Let us now look at the links between this isotropy of the signal and the spin transport parameters. The absorbed spin current  $J_c$  is converted into a charge current  $J_s$  according to  $J_c = \theta J_s$ . Importantly,  $\theta$  is not the sole figure of merit of the ISHE. The conversion indeed occurs only over a limited material thickness, roughly equal to the spin-relaxation length, after which the spin current, which is not conserved, vanishes. The produced signal is, thus, actually proportional to the product of the spin Hall angle by the spin-relaxation length. If the incoming spins are collinear to the magnetization, this product is  $\theta_{\parallel} l_{sf}$ , where  $\theta_{\parallel}$  is the spin Hall angle in the collinear situation. If the incoming spins are transverse to the magnetization, this product becomes  $\theta_{\perp}$  times  $\lambda_{\perp}$  with  $\lambda_{\perp}$  as the transverse spin-relaxation length.  $\lambda_{\perp}$  represents the ballistic relaxation by phase averaging of the spin current with a polarization transverse to the magnetization. The isotropy of the ISHE signal suggests that in our experiments,

$$\theta_{\parallel} l_{sf} \sim \theta_{\perp} \lambda_{\perp}. \quad (2)$$

In principle, it is possible to measure separately  $l_{sf}$  and  $\lambda_{\perp}$  as they affect the spin absorption [44].  $l_{sf}$  has been measured in NiCu [27] and is equal to 2.4 nm at room temperature. The measurement of  $\lambda_{\perp}$  is more complex. The presence of a large interface resistance prevents here the observation of the spin absorption anisotropy in our devices. It also has the effect of keeping the amount of spin current contributing to the ISHE constant. Extracting  $\lambda_{\perp}$  would require the thickness-dependence measurement [31] with all the spurious effects linked film thickness reduction [50].

An estimation of  $\lambda_{\perp}$  can be obtained by assuming that it is inversely proportional to the exchange interaction [51] and, thus, to the Curie temperature [52]. By taking as a reference material Py, which has a  $T_c$  of 800 K [53] with  $\lambda_{\perp}^{\text{Py}} \sim 1$  nm [44,51],  $\lambda_{\perp}$  in NiCu can be estimated to be  $\lambda_{\perp}^{\text{NiCu}} \sim 5$  nm. The transverse relaxation length due to ballistic effects in NiCu is, therefore, larger than its spin-diffusion length. This means that the transverse spin current relaxes mainly over the spin-diffusion length through diffusive processes and that  $\lambda_{\perp}^{\text{NiCu}} = l_{sf}$  so that  $\theta_{\perp} = \theta_{\parallel}$  according to our experimental result of Eq. (2). The case of NiPd is more difficult to analyze since we do not have values for its spin-diffusion length. However, we may expect the same isotropic behavior of the interconversion observed in NiCu as will be discussed later on.

The isotropy of the spin current relaxation lengths in ferromagnetic NiCu contrasts with the observation of a large spin-relaxation anisotropy in high- $T_c$  ferromagnets, such as NiFe, Co, and CoFe [44]. The possibility for a spin current to exist in the bulk of a ferromagnetic material in the presence of a sizable SO interaction with respect to the exchange interaction, might be due to the presence of non-collinear spin eigenstates at avoided crossings between bands of opposite spin [17]. Such a relation between the SO and the exchange interaction appears to be realized in NiCu and NiPd. Indeed, the large measured spin and anomalous Hall angles point toward a large SO interaction, whereas the low  $T_c$  indicates a low exchange interaction. This situation contrasts strongly with the one explored in Ref. [44] and would explain the observed spin-relaxation isotropy in both NiCu and NiPd. Previous publications [17,18] analyzed the anisotropy of the SHE in ferromagnetic materials in terms of the superposition of an isotropic SHE to which is added the so-called spin anomalous effect, which originates from the polarization of the charge current produced by the anomalous Hall effect. Our results indicates here that, despite the large anomalous Hall angles in NiCu and NiPd, this effect does not contribute to the interconversion. Furthermore, this happens for materials in which the interconversion is expected to be driven by the intrinsic (NiCu) [36] and the extrinsic effect (NiPd) [35], and despite the previous observation of a link between the extrinsic anomalous and spin Hall effects [11].

To conclude, we proposed a device allowing the measurement of the anisotropy of the spin-charge interconversion in ferromagnetic materials. Although the paramagnetic/ferromagnetic transition is associated with symmetry breaking, the ISHE signal in NiCu and NiPd remains surprisingly independent of the magnetization direction in the ferromagnetic phase. In terms of spin transport properties, this implies that the product of the SHA by the

spin-relaxation length is the same in the collinear and transverse configuration. In the studied low  $T_c$  materials, this can be understood by the long transverse relaxation length which causes the spin current to relax during scattering on SO impurities and, therefore, to be equal to the spin-diffusion length.

A thorough understanding of the relation between the SO and the exchange interactions on the spin-charge interconversion anisotropy will require a more systematic investigation using our new geometry of the lateral spin valve, and the observation of the isotropy of the spin-relaxation length and spin Hall angles in  $\text{Ni}_{60}\text{Cu}_{40}$  and  $\text{Ni}_{16}\text{Pd}_{84}$  as a starting point. This can be achieved by changing the relative strength of the

SO and exchange interaction by modifying the composition of these two alloys.

The data associated to the figures can be found at the following link in Ref. [66]

We acknowledge support from the Institut Universitaire de France, from the Project CONTRABASS under Grant Agreements No. ANR-20-CE24-0023 from the Agence Nationale de la Recherche, and from the SPEAR ITN. This project also received funding from the European Union's Horizon 2020 research and innovation program under the Marie Skłodowska-Curie Grant Agreement No. 955671.

- 
- [1] T. Valet and A. Fert, Theory of the perpendicular magnetoresistance in magnetic multilayers, *Phys. Rev. B* **48**, 7099 (1993).
- [2] M. D. Stiles and A. Zangwill, Anatomy of spin-transfer torque, *Phys. Rev. B* **66**, 014407 (2002).
- [3] Q. Shao, P. Li, L. Liu, H. Yang, S. Fukami, A. Razavi, H. Wu, K. Wang, F. Freimuth, Y. Mokrousov, M. D. Stiles, S. Emori, A. Hoffmann, J. Akerman, K. Roy, J.-P. Wang, S.-H. Yang, K. Garello, and W. Zhang, Roadmap of spinorbit torques, *IEEE Trans. Magn.* **57**, 800439 (2021).
- [4] S. Manipatruni, D. E. Nikonov, C.-C. Lin, T. A. Gosavi, H. Liu, B. Prasad, Y.-L. Huang, E. Bonturim, R. Ramesh, and I. A. Young, Scalable energy-efficient magnetoelectric spin-orbit logic, *Nature (London)* **565**, 35 (2019).
- [5] J. Sinova, S. O. Valenzuela, J. Wunderlich, C. H. Back, and T. Jungwirth, Spin Hall effects, *Rev. Mod. Phys.* **87**, 1213 (2015).
- [6] Y. K. Kato, C. Myers, C. Gossard, and D. D. Awschalom, Observation of the Spin Hall Effect in Semiconductors, *Science* **306**, 1910 (2004).
- [7] Y. Tserkovnyak, A. Brataas, and G. E. W. Bauer, Spin pumping and magnetization dynamics in metallic multilayers, *Phys. Rev. B* **66**, 224403 (2002).
- [8] P. Laczkowski, M. Cosset-Cheneau, W. Savero-Torres, V. T. Pham, G. Zahnd, H. Jaffrès, N. Reyren, J.-C. Rojas-Sanchez, A. Marty, L. Vila, J.-M. George, and J.-P. Attané, Spin-dependent transport characterization in metallic lateral spin valves using one-dimensional and three-dimensional modeling, *Phys. Rev. B* **99**, 134436 (2019).
- [9] L. Liu, T. Moriyama, D. C. Ralph, and R. A. Buhrman, Spin-Torque Ferromagnetic Resonance Induced by the Spin Hall Effect, *Phys. Rev. Lett.* **106**, 036601 (2011).
- [10] Y.-T. Chen, S. Takahashi, H. Nakayama, M. Althammer, S. T. B. Goennenwein, E. Saitoh, and G. E. W. Bauer, Theory of spin Hall magnetoresistance, *Phys. Rev. B* **87**, 144411 (2013).
- [11] Y. Omori, E. Sagasta, Y. Niimi, M. Gradhand, L. E. Hueso, F. Casanova, and Y. C. Otani, Relation between spin Hall effect and anomalous Hall effect in 3d ferromagnetic metals, *Phys. Rev. B* **99**, 014403 (2019).
- [12] O. Gladii, L. Frangou, A. Hallal, R. L. Seeger, P. Noël, G. Forestier, S. Auffret, M. Rubio-Roy, P. Warin, L. Vila, S. Wimmer, H. Ebert, S. Gambarelli, M. Chshiev, and V. Baltz, Self-induced inverse spin Hall effect in ferromagnets: Demonstration through nonmonotonic temperature dependence in permalloy, *Phys. Rev. B* **100**, 174409 (2019).
- [13] T. Taniguchi, J. Grollier, and M. D. Stiles, Spin-Transfer Torque Generated by the Anomalous Hall Effect and Anisotropic Magnetoresistance, *Phys. Rev. Appl.* **3**, 044001 (2015).
- [14] M. Kimata, H. Chen, K. Kondou, S. Sugimoto, P. K. Muduli, M. Ikhlas, Y. Omori, T. Tomita, A. H. MacDonald, S. Nakatsuji, and Y. Otani, Magnetic and magnetic inverse spin Hall effects in a non-collinear antiferromagnet, *Nature (London)* **565**, 627 (2019).
- [15] Y. Hibino, T. Taniguchi, K. Yakushiji, A. Fukushima, H. Kubota, and S. Yuasa, Giant charge-to-spin conversion in ferromagnet via spin-orbit coupling, *Nat. Commun.* **12**, 6254 (2021).
- [16] A. Davidson, V. P. Amin, W. S. Aljuaid, P. M. Haney, and X. Fan, Perspectives of electrically generated spin currents in ferromagnetic materials, *Phys. Lett. A* **384**, 126228 (2020).
- [17] V. P. Amin, Junwen Li, M. D. Stiles, and P. M. Haney, Intrinsic spin currents in ferromagnets, *Phys. Rev. B* **99**, 220405(R) (2019).
- [18] K. S. Das, W. Y. Schoemaker, B. J. van Wees, and I. J. Vera-Marun, Spin injection and detection via the anomalous spin Hall effect of a ferromagnetic metal, *Phys. Rev. B* **96**, 220408(R) (2017).
- [19] T. Wimmer, B. Coester, S. Geprag, R. Gross, S. T. B. Goennenwein, H. Huebl, and M. Althammer, Anomalous spin Hall angle of metallic ferromagnet determined by a multiterminal spin injection/detection device, *Appl. Phys.* **115**, 092404 (2019).
- [20] D. Tian, Y. Li, D. Qu, S. Y. Huang, X. Jin, and C. L. Chien, Manipulation of pure spin current in ferromagnetic metals independent of magnetization, *Phys. Rev. B* **94**, 020403(R) (2016).
- [21] K. Ando, S. Takahashi, J. Ieda, Y. Kajiwara, H. Nakayama, T. Yoshino, K. Harii, Y. Fujikawa, M. Matsuo, S. Maekawa, and E. Saitoh, Inverse spin-Hall effect induced by spin pumping in metallic system, *J. Appl. Phys.* **109**, 103913 (2011).
- [22] V. T. Pham, L. Vila, G. Zahnd, A. Marty, W. Savero-Torres, M. Jamet, and J. P. Attane, Ferromagnetic/nonmagnetic nanostructures for the electrical measurement of the spin Hall effect, *Nano Lett.* **16**, 6755 (2016).
- [23] S. O. Valenzuela and M. Tinkham, Direct electronic measurement of the spin Hall effect, *Nature (London)* **442**, 176 (2006).

- [24] J. Kim, P. Sheng, S. Takahashi, S. Mitani, and M. Hayashi, Spin Hall Magnetoresistance in Metallic Bilayers, *Phys. Rev. Lett.* **116**, 097201 (2016).
- [25] K. Uchida, S. Takahashi, K. Harii, J. Ieda, W. Koshibae, K. Ando, S. Maekawa, and E. Saitoh, Observation of the spin Seebeck effect, *Nature (London)* **455**, 778 (2008).
- [26] M. Hayashi, J. Kim, M. Yamanouchi, and H. Ohno, Quantitative characterization of the spin-orbit torque using harmonic Hall voltage measurements, *Phys. Rev. B* **89**, 144425 (2014).
- [27] S. Varotto, M. Cosset-Chéneau, C. Grezes, Y. Fu, P. Warin, A. Brenac, J.-F. Jacquot, S. Gambarelli, C. Rinaldi, V. Baltz, J.-P. Attané, L. Vila, and P. Noel, Independence of the Inverse Spin Hall Effect with the Magnetic Phase in Thin NiCu Films, *Phys. Rev. Lett.* **125**, 267204 (2020).
- [28] Y. Ou, Z. Wang, C. S. Chang, H. P. Nair, H. Paik, N. Reynolds, D. C. Ralph, D. A. Muller, D. G. Schlom, and R. A. Buhrman, Exceptionally High, Strongly Temperature Dependent, Spin Hall Conductivity of SrRuO<sub>3</sub>, *Nano Lett.* **19**, 3663 (2019).
- [29] J. D. Gibbons, D. MacNeill, R. A. Buhrman, and D. C. Ralph, Reorientable Spin Direction for Spin Current Produced by the Anomalous Hall Effect, *Phys. Rev. Appl.* **9**, 064033 (2018).
- [30] B. F. Miao, S. Y. Huang, D. Qu, and C. L. Chien, Inverse Spin Hall Effect in a Ferromagnetic Metal, *Phys. Rev. Lett.* **111**, 066602 (2013).
- [31] Z. Zhu, X. Zheng, G. Li, H. Bai, J. Su, Y. Zhang, and J.-W. Cai, Strong spin orientation-dependent spin current diffusion and inverse spin Hall effect in a ferromagnetic metal, *NPG Asia Mater.* **12**, 12 (2020).
- [32] H. Mizuno, H. Isshiki, K. Kondou, Y. Zhu, and Y. Otani, Influence of planar Hall effect on the output signal in a T-shaped spin conversion device, *Appl. Phys. Lett.* **119**, 092401 (2021).
- [33] I. Groen, V. T. Pham, N. Leo, A. Marty, L. E. Hueso, and F. Casanova, Disentangling Spin, Anomalous, and Planar Hall Effects in Ferromagnet-Heavy-Metal Nanostructures, *Phys. Rev. Appl.* **15**, 044010 (2021).
- [34] J. Cramer, A. Ross, S. Jaiswal, L. Baldrati, R. Lebrun, and M. Klaui, Orientation-dependent direct and inverse spin Hall effects in Co<sub>60</sub>Fe<sub>20</sub>B<sub>20</sub>, *Phys. Rev. B* **99**, 104414 (2019).
- [35] D. H. Wei, Y. Niimi, B. Gu, T. Ziman, S. Maekawa, and Y. Otani, The spin Hall effect as a probe of nonlinear spin fluctuations, *Nat. Commun.* **3**, 1058 (2012).
- [36] M. W. Keller, K. S. Gerace, M. Arora, E. K. Delczeg-Czirjak, J. M. Shaw, and T. J. Silva, Near-unity spin Hall ratio in NiCu alloys, *Phys. Rev. B* **99**, 214411 (2019).
- [37] G. Zahnd, L. Vila, V. T. Pham, M. Cosset-Chéneau, W. Lim, A. Brenac, P. Laczkowski, A. Marty, and J. P. Attané, Spin diffusion length and polarization of ferromagnetic metals measured by the spin-absorption technique in lateral spin valves, *Phys. Rev. B* **98**, 174414 (2018).
- [38] See Supplemental Material at <http://link.aps.org/supplemental/10.1103/PhysRevB.106.L220405> which includes Refs. [16,17,27,37,39,44,48,51,54–65].
- [39] Y. Niimi and Y. Otani, Reciprocal spin Hall effects in conductors with strong spin-orbit coupling: A review, *Rep. Prog. Phys.* **78**, 124501 (2015).
- [40] J.-C. Rojas Sánchez, P. Laczkowski, W. F. Saverio Torres, M. Cubukcu, V. D. Nguyen, L. Notin, C. Beigné, C. Vergnaud, A. Marty, M. Jamet, L. Vila, and J. P. Attané, In-plane and out-of-plane spin precession in lateral spin-valves, *Appl. Phys. Lett.* **102**, 132408 (2013).
- [41] G. Zahnd, L. Vila, V. T. Pham, F. Rortais, M. Cosset-Chéneau, C. Vergnaud, M. Jamet, P. Noel, T. Gushi, A. Brenac, A. Marty, and J. P. Attané, Observation of the Hanle effect in giant magnetoresistance measurements, *Appl. Phys. Lett.* **112**, 232405 (2018).
- [42] G. Zahnd, L. Vila, T. V. Pham, A. Marty, P. Laczkowski, W. Saverio Torres, C. Beigné, C. Vergnaud, M. Jamet, and J.-P. Attané, Comparison of the use of NiFe and CoFe as electrodes for metallic lateral spin valves, *Nanotechnology* **27**, 035201 (2016).
- [43] L. Vila, T. Kimura and Y.C. Otani, Evolution of the Spin Hall Effect in Pt Nanowires: Size and Temperature Effects, *Phys. Rev. Lett.* **99**, 226604 (2007).
- [44] M. Cosset-Chéneau, L. Vila, G. Zahnd, D. Gusakova, V. T. Pham, C. Grezes, X. Waintal, A. Marty, H. Jaffres, and J.-P. Attané, Measurement of the Spin Absorption Anisotropy in Lateral Spin Valves, *Phys. Rev. Lett.* **126**, 027201 (2021).
- [45] A. Brataas, G. E. W. Bauer, and P. J. Kelly, Non-collinear magnetoelectronics, *Phys. Rep.* **427**, 157 (2006).
- [46] A. P. Mihai, J. P. Attané, A. Marty, P. Warin, and Y. Samson, Electron-magnon diffusion and magnetization reversal detection in FePt thin films, *Phys. Rev. B* **77**, 060401(R) (2008).
- [47] V. D. Nguyen, L. Vila, P. Laczkowski, A. Marty, T. Faivre, and J. P. Attané, Detection of Domain-Wall Position and Magnetization Reversal in Nanostructures Using the Magnon Contribution to the Resistivity, *Phys. Rev. Lett.* **107**, 136605 (2011).
- [48] H. Z. Arham, T. S. Khaire, R. Loloee, W. P. Pratt, Jr., and N. O. Birge, Measurement of spin memory lengths in PdNi and PdFe ferromagnetic alloys, *Phys. Rev. B* **80**, 174515 (2009).
- [49] G. Qu, K. Nakamura, and M. Hayashi, Magnetization direction dependent spin Hall effect in 3d ferromagnets, *Phys. Rev. B* **102**, 144440 (2020).
- [50] C. Gonzalez-Fuentes, R. Henriquez, C. Garcia, R. K. Dumas, B. Bozzo, and A. Pomar, Spin diffusion length associated with out-of-plane conductivity of Pt in spin pumping experiments, *Phys. Rev. B* **103**, 224403 (2021).
- [51] C. Petitjean, D. Luc, and X. Waintal, Unified Drift-Diffusion Theory for Transverse Spin Currents in Spin Valves, Domain Walls, and Other Textured Magnets, *Phys. Rev. Lett.* **109**, 117204 (2012).
- [52] I. Turek, J. Kudrnovsky, V. Drchal and P. Bruno, Exchange interactions, spin waves, and transition temperatures in itinerant magnets, *Philos. Mag.* **86**, 1713 (2006).
- [53] X. Zhang, Y. Lao, J. Sklenar, N. S. Bingham, J. T. Batley, J. D. Watts, C. Nisoli, C. Leighton, and P. Schiffer, Understanding thermal annealing of artificial spin ice, *APL Mater.* **7**, 111112 (2019).
- [54] A. J. Wright, M. J. Erickson, D. Bromley, P. A. Crowell, C. Leighton, and L. O'Brien, Origin of the magnetic field enhancement of the spin signal in metallic nonlocal spin transport devices, *Phys. Rev. B* **104**, 014423 (2021)
- [55] C. Qin, S. Chen, Y. Cai, F. Kandaz, and Y. Ji, Nonlocal electrical detection of spin accumulation generated by anomalous Hall effect in mesoscopic Ni<sub>81</sub>Fe<sub>19</sub> films, *Phys. Rev. B* **96**, 134418 (2017)
- [56] W. Saverio Torres, P. Laczkowski, V. D. Nguyen, J. C. Rojas Sanchez, L. Vila, A. Marty, M. Jamet, and J. P. Attané, Switchable Spin-Current Source Controlled by Magnetic Domain Walls, *Nano Lett.* **14**, 4016 (2014)

- [57] P. Laczkowski, H. Jaffres, W. Savero-Torres, J.-C. Rojas-Sanchez, Y. Fu, N. Reyren, C. Deranlot, L. Notin, C. Beigné, J.-P. Attané, L. Vila, J.-M. George, and A. Marty, Evaluation of spin diffusion length of AuW alloys using spin absorption experiments in the limit of large spin-orbit interactions, *Phys. Rev. B* **92**, 214405 (2015).
- [58] C. Geuzaine and J.-F. Remacle, Gmsh: A three-dimensional finite element mesh generator with built-in pre- and post-processing facilities, *Int. J. Numer. Meth. Engng.* **79**, 1309 (2009).
- [59] P. Dular, C. Geuzaine, A. Genon, and W. Legros, An evolutive software environment for teaching finite element methods in electromagnetism, *IEEE Trans. Magn.* **35**, 1682 (1999).
- [60] E. Sagasta, Y. Omori, M. Isasa, M. Gradhand, L. E. Hueso, Y. Niimi, Y. C. Otani, and F. Casanova, Tuning the spin Hall effect of Pt from the moderately dirty to the superclean regime, *Phys. Rev. B* **94**, 060412(R) (2016).
- [61] L. Liu, R. A. Buhrman, and D. C. Ralph, Review and Analysis of Measurements of the Spin Hall Effect in Platinum, [arXiv:1111.3702](https://arxiv.org/abs/1111.3702).
- [62] V. T. Pham, M. Cosset-Chéneau, A. Brenac, O. Boulle, A. Marty, J.-P. Attané, and L. Vila, Evidence of interfacial asymmetric spin scattering at ferromagnet-Pt interfaces, *Phys. Rev. B* **103**, L201403 (2021).
- [63] J. Bass, Jr. and W. P. Pratt, Spin-diffusion lengths in metals and alloys, and spin-flipping at metal/metal interfaces: An experimentalist's critical review, *J. Phys.: Condens. Matter* **19**, 183201 (2007).
- [64] R. S. Nair, E. Barati, K. Gupta, Z. Yuan, and P. J. Kelly, Spin-Flip Diffusion Length in 5d Transition Metal Elements: A First-Principles Benchmark, *Phys. Rev. Lett.* **126**, 196601 (2021).
- [65] W. S. Torres, A. Marty, P. Laczkowski, M. Jamet, L. Vila, and J.-P. Attané, Calculation method of spin accumulations and spin signals in nanostructures using spin resistors, *Eur. Phys. J. B* **91**, 37 (2018).
- [66] <https://doi.org/10.57745/Z3BG2U>.